The Microphysical Structure and Evolution of Hawaiian Rainband Clouds. Part II: Aircraft Measurements within Rainbands Containing High Reflectivity Cores

MARCIN J. SZUMOWSKI

Illinois State Water Survey, Champaign, Illinois, and Department of Atmospheric Sciences, University of Illinois at Urbana–Champaign, Urbana, Illinios

ROBERT M. RAUBER

Department of Atmospheric Sciences, University of Illinois at Urbana–Champaign, Urbana, Illinois

HARRY T. OCHS III* AND KENNETH V. BEARD

Illinois State Water Survey, Champaign, Illinois, and Department of Atmospheric Sciences, University of Illinois at Urbana–Champaign, Urbana, Illinios

(Manuscript received 11 October 1996, in final form 27 May 1997)

ABSTRACT

The microphysical structure of high reflectivity cores and surrounding weaker echo regions in Hawaiian rainbands is documented using aircraft data. These data show that high reflectivity cores are associated with giant raindrops ($D > 4$ mm) present in narrow ($\sim$500 m wide) columns coincident with the core updraft. Updrafts were found to be strong enough to suspend 1–2-mm raindrops near cloud top. As these raindrops subsequently fall through the updraft core, they are exposed to high liquid water content, allowing them to grow to large sizes, provided that updrafts are not significantly sheared. The data indicate that size sorting due to differential terminal velocities of the larger and smaller raindrops occurs initially in the updraft. As a result, the larger raindrops fall through an environment in which there is a low concentration of smaller raindrops, decreasing the probability of breakup. Calculations of raindrop growth rates and breakup probabilities are used to demonstrate that high reflectivity cores in the rainbands can result from simple accretional growth of 1–2-mm raindrops falling from cloud top. In regions outside of the main updraft, drop size distributions were approximately exponential, with higher concentrations of small raindrops and no giant raindrops. Consequently radar reflectivities and rainfall rates were lower. In these regions, collisional breakup played a more significant role in eliminating the large size tail of the spectra.

1. Introduction

The warm rain process is responsible for much of the rain in the Tropics and contributes to precipitation formation in many midlatitude convective clouds (Saunders 1965; Carbone and Nelson 1978; Johnson 1982; Illingworth 1988; Beard and Ochs 1993). Despite numerous observational, laboratory, and modeling studies, several aspects of warm rain formation are still subjects of debate. It is unclear whether stochastic processes (Telford 1955, 1975; Gillespie 1972; Berry and Reinhardt 1974) are necessary to initiate precipitation embryos, or as Ochs and Semonin (1979) and Johnson (1982) hypothesized, rain formation can begin directly from condensation on ultragiant nuclei (Woodcock 1952, 1953; Johnson 1976; Ochs and Gatz 1980). Another open question is the role of small-scale cloud circulations in enhancing rapid development of precipitation within convective updrafts. Johnson (1982) used three different Lagrangian parcel models to argue that raindrops can grow large enough to produce reflectivity factors greater than 40 dBZ in 15–30 min during a simple up–down trajectory through a cloud with a 2 m s^{-1} updraft with adiabatic liquid water content. Beard et al. (1986) and Johnson et al. (1986) subsequently demonstrated, using a Bowen (1950) model, that large raindrops could grow in shallow clouds in realistic time frames from initial ultragiant nuclei. Alternatively, Rauber et al. (1991), using aircraft data collected during the Joint Hawaiian Warm Rain Project (Beard et al. 1986; Takahashi et al. 1989), suggested that a recirculation mechanism may occur near cloud-top regions that

Corresponding author address: Marcin J. Szumowski, Department of Atmospheric Sciences, University of Illinois, 105 S. Gregory Ave., Urbana, IL 61801.
E-mail: marcin@atmos.uiuc.edu

can accelerate raindrop growth by transporting drops into favorable regions for accretional growth. Observations are required to examine hypotheses and validate existing models of warm rain formation. Detailed studies that document the evolution of the reflectivity, kinematic, and microphysical structure of clouds that produce rain solely through warm processes have been unavailable in the literature.

The tropical, maritime environment off the windward shore of the Big Island of Hawaii provides an ideal natural laboratory to study warm rain processes. Shallow rainbands commonly form offshore of the island (Austin et al. 1996) and are enhanced by convergence associated with flow deformation (Smolarkiewicz et al. 1988; Carbone et al. 1996). Hawaiian rainbands, despite their shallow depth, develop very heavy rainfall on short timescales (Szumowski et al. 1997, hereafter Part I). Raindrops with equivalent spherical diameters between 4 and 8 mm have been recorded in rain shafts of some of the more vigorous cells (Beard et al. 1986). These precipitation shafts produce very high radar reflectivity factors (>50 dBZ). Convective updrafts as strong as 10 m s^{-1} were found to precede the development of individual high reflectivity cores. Based on the temporal evolution of the high reflectivity cores and the corresponding updrafts, and the vertical structure and spatial relationships between maximum updrafts and peak reflectivity, it was inferred (Part I) that the most rapid raindrop growth occurs near cloud tops where sharp reflectivity gradients were observed. In some cases, persistent, strong (>7 m s^{-1}) updrafts led to formation of very high (>60 dBZ) reflectivities near cloud top, indicating the presence of giant raindrops at the trade wind inversion level.

This paper is the second in a series describing the structure and evolution of high reflectivity cores observed by aircraft and radars in Hawaiian rainbands. In this paper, we 1) present aircraft measurements to document the microphysical structure of high reflectivity cores and surrounding regions of Hawaiian rainbands, 2) relate the microphysical structure of the clouds to the radar measurements presented in Part I, and 3) present calculations that demonstrate that high reflectivity cores in the rainbands can result from simple accretional growth of raindrops provided that vertical wind shear is minimal and that size sorting due to differential fall velocity occurs within the stronger updrafts.

2. Overview of aircraft data

Data presented in this paper were collected during the Joint Hawaiian Warm Rain Project (JHWRP) in 1985 and the Hawaiian Rainband Project (HaRP) in 1990. The University of Wyoming (UW) King Air was the source of kinematic and microphysical data in rainbands during JHWRP. HaRP used the 5-cm wavelength National Center for Atmospheric Research CP3 and CP4 Doppler radar systems as well as the NCAR Electra aircraft. A map of Hawaii including the locations of the radars used in HaRP is shown in Fig. 1.

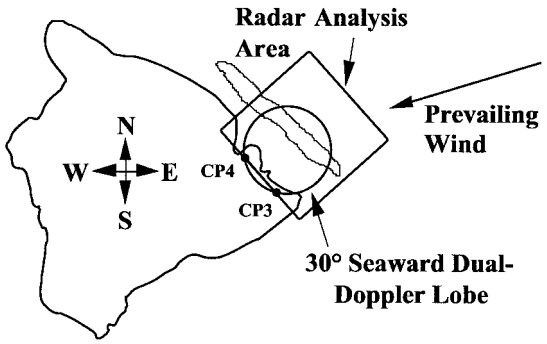

FIG. 1. Island of Hawaii showing the seaward 30° dual-Doppler lobe, the radar analysis area, and the location of the CP3 and CP4 radars.

The aircraft used in JHWRP and HaRP carried similar instrumentation. During JHWRP, the University of Wyoming King Air was equipped with a 100-μm resolution two-dimensional precipitation (2D-P) optical array probe (OAP), a 25-μm resolution two-dimensional cloud (2D-C) OAP, a forward scattering spectrometer probe (FSSP), and a 260X probe (Beard et al. 1986; Rauber et al. 1991). During HaRP, the NCAR Electra carried two out of three of the following OAPs on any given flight: a 200-μm resolution 2D-P OAP, a 100-μm resolution 2D-P OAP, and a 25-μm resolution 2D-C OAP. An FSSP and a 260X probe were also flown. The OAPs were located on the wing tips of the King Air, but were mounted on the fuselage of the Electra. Flow around the Electra fuselage distorted raindrop shapes and caused breakup of all raindrops larger than about 3 mm (Rogers 1990). As a result, large raindrops, frequently sampled during JHWRP, were completely absent from the HaRP data.

In addition to the breakup problem caused by the unfortunate OAP probe location on its fuselage, the Electra had a broad range of missions during HaRP leaving only part of the flight time for cloud microphysical studies. The location of cloud penetrations during HaRP was coordinated at CP4. A several minute time lag typically occurred between the time that a high reflectivity region was identified and the time that the aircraft would arrive at the targeted position. The advection and rapid evolution of the high reflectivity regions during the time required for the aircraft to arrive at the target often caused the aircraft to miss the high reflectivity region. Our survey of the complete HaRP dataset showed that the Electra penetrated only one high reflectivity (>50 dBZ) region of a rainband during the entire project.

During JHWRP, the King Air, a smaller aircraft, was primarily used for cloud microphysical studies. Selected flights were targeted through high reflectivity regions of rainbands using the onboard cockpit radar. Although high reflectivity regions of rainbands were frequently

sampled, only two cases, 23 July 1985 and 19 July 1985, were available for which the entire life cycle of a high reflectivity region was documented through the depth of the rainband. With two exceptions, all of the other 17 cases we examined involved penetrations of high reflectivity regions at or below cloud base. The two cases that were exceptions during JHWRP involved bands associated with synoptic-scale disturbances. The first was a rainband that extended over a thousand miles from the intertropical convergence zone into the midlatitudes (Takahashi et al. 1989). The second was a rainband that was influenced by Hurricane Ignatio. In both of these cases the clouds extended above the freezing level and contained ice, and therefore did not conform to the summertime pattern of rainband development typically observed off the windward shore of Hawaii (Austin et al. 1996).

From the complete JHWRP and HaRP datasets, we chose to present the 19 July 1985 and 23 July 1985 case studies from JHWRP since these cases provide the most comprehensive view of the microphysical structure of high reflectivity cores in Hawaiian rainbands. We relate JHWRP aircraft data for the 23 July 1985 and 19 July 1985 cases to HaRP dual-Doppler radar measurements. Comparison of the 1985 aircraft with 1990 radar data was necessitated by the problems with the Electra data, but is justified since the structure of shallow summertime convection near the windward shore of the Big Island of Hawaii does not vary significantly. Nevertheless, to ensure that cases from the two projects are indeed similar, the thermodynamic structure of the trade wind layer and cloud characteristics will be compared (section 3a). Methods for processing the radar equivalent reflectivity factor (hereafter called reflectivity) and velocity fields were discussed in Part I. For convenience, we use the terminology introduced in Part I: the term ''rainband'' will refer to either a continuous or broken elongated region of precipitation (radar reflectivity); a ''cell'' will refer to a locally higher region of radar reflectivity, either isolated, or embedded within a rainband; and a ''high reflectivity core'' will refer to a local region of reflectivity exceeding 50 dBZ.

All OAP data presented in this paper were carefully processed and hand edited to remove artifacts using the image processing software discussed by Rauber et al. (1995). Raindrop sizes are reported as equivalent spherical diameter (D). Liquid water contents were measured by the Johnson–Williams (JW) hot wire device. Radar reflectivity factors and rainfall rates were calculated from the 2D-P OAP raindrop spectra (Rogers and Yau 1989, 182 and 190), with a correction applied to account for the increase in reflectivity that occurs for horizontally polarized radars such as CP3 and CP4 due to the oblate shape of large raindrops (Doviak and Zrnić 1993, 249). Calculated reflectivities and rainfall rates should be considered qualitative because the small sample volume ($\sim$1 m^3) of the 2DP OAP leads to poor counting statistics for the very large drops (Cornford 1967).

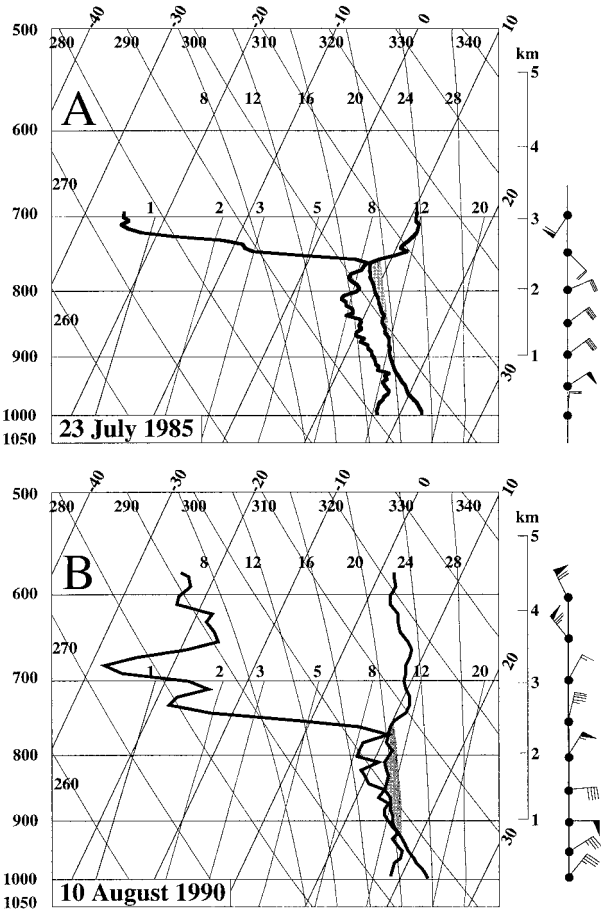

FIG. 2. Thermodynamic diagrams showing soundings taken upstream of the island by (a) the UW King Air on 23 July 1985 at approximately 1615 UTC; (b) the NCAR Electra on 10 August 1990 at approximately 1620 UTC. The shaded areas indicate the convective available potential energy (CAPE). A barb and pennant, respectively, represent wind speeds of 1 and 5 m s^{-1}.

3. Observations

a. 23 July 1985

The time evolution, spatial dimensions, structure, and calculated reflectivity within the rain shaft that developed in a cell on 23 July 1985 corresponded closely to features observed with radar in the high reflectivity cores discussed in Part I. The 23 July cell developed an intense rain shaft containing very large raindrops and an anvil-like overhang region of precipitation on the flanks of the rain shaft as air diverged out of the updraft region near the inversion.

The sounding from 23 July 1985 (Fig. 2a), taken just upwind of the island, had a mixed layer extending from the surface to approximately 500 m, a lifting condensation level (LCL) at 750 m, and a level of free convection (LFC) at 995 m. The trade wind layer was conditionally unstable with a convective available potential energy (CAPE) of 52 J kg^{-1}, corresponding to a maximum possible adiabatic updraft of 10.2 m s^{-1}. A 3.8°C

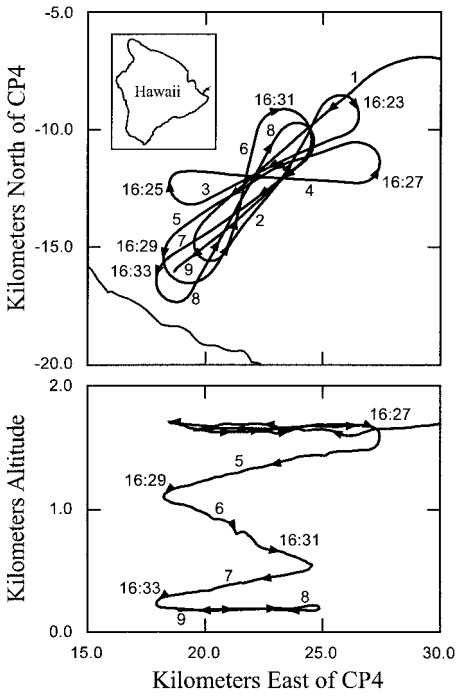

FIG. 3. The UW King Air horizontal (top) and vertical (bottom) flight track on 23 July 1985 between 1618 and 1637 UTC.

inversion, located between 2350 m and 2520 m, limited the vertical development of the convection. The trade winds below the inversion were about 4 m s^{-1} from the northeast.

Multilevel penetrations of a cell were made over a 20-min period during the early and mature stages of the cell's development. Each pass was targeted through the region of highest reflectivity, as determined from the onboard radar. Figure 3, the horizontal and vertical flight track between 1618:00 and 1637:15 UTC shows the locations and elevations of the cloud passes. The origin of the coordinate system in Fig. 3 is the HaRP CP4 radar location. For convenience, this reference frame was used for all our JHWRP and HaRP analyses, although the radars were only involved in the HaRP project (Fig. 1). Data collected during nine cloud passes between 1618:50 and 1637:15 UTC are shown in Figs. 4a–c. Passes 10–13 (not shown) were similar to pass 9 and were made at the same level. Each panel displays 60 seconds of data, equivalent to a distance of approximately 6 km along the flight track. The data are presented so that the left side of each panel is at the southeast end of a pass. The data from each pass are displayed in two panels, the first (following Johnson et al. 1986) showing the size and time of each precipitation drop measured by the 100-μm resolution 2D-P OAP, and the second showing the vertical motion and the liquid water content. Figures 4a and 4b also show cloud droplet spectra within the high liquid water content regions (denoted i–v) averaged over about 1.0 km. Figures 4a–c also show raindrop spectra averaged over 1 km for selected regions of the rainband (denoted I–XV). Reflectivity values and rainfall rates appearing in individual panels were calculated from the raindrop spectra.

Passes 1–4 were flown at 1700 m, 600 m below the base of the inversion. The updraft during each pass was ~2 km wide with a central core 0.6–0.9 km wide where vertical velocities exceeded 4 m s^{-1}. The peak vertical velocities ranged from 7.5 to 9.5 m s^{-1}. Comparison with the maximum vertical velocity estimated from the CAPE (Fig. 2a) suggests that the updraft core should have been nearly adiabatic. However, the peak liquid water content observed during each of the four passes ranged from 1.0 to 1.2 g m^{-3}, about half of the adiabatic value at 1700 m. There was a direct correspondence between the vertical motion and the liquid water content fields during each pass. Cloud droplet concentrations within regions i–iv ranged from 70 to 110 cm^{-3} in the updraft core but were lower (20–40 cm^{-3}) in the cloud outside of the main updraft. The mode of the cloud droplet spectra was ~25 μm in regions i–iv and cloud droplets with diameters between 30 and 48 μm were present within the updraft in concentrations up to 8 cm^{-3}.

During the first pass, a few raindrops as large as 1 mm were observed, but most raindrops were smaller than 0.5 mm. Raindrops were detected in two areas, within the downdraft on the northeast side of the cell and on the southwest side of the updraft. No raindrops were detected within a region ~500 m wide on the northwest side of the updraft. During passes 2–4, raindrops were observed over a wider region. Most raindrops were smaller than 1 mm, and the lowest raindrop concentrations were coincident with the updraft core. Raindrops with sizes exceeding 1 mm were generally observed in regions of weaker updraft and in downdraft areas. Small raindrops were notably absent in the high liquid water content updraft core of pass 4. Also notable are the large 4.9 and 3.4 mm drops within the main updraft. Reflectivities calculated from the raindrop spectra in regions I–III in passes 2–3 were <25 dBZ. By the time of pass 4, the calculated reflectivity within the updraft (region IV) had increased to 45 dBZ as larger raindrops continued to form.

Passes 5–7 were at the nominal elevations of 1300, 900, and 400 m as the aircraft descended. Pass 7 was below cloud base. The main updraft in pass 5 was 800 m wide and peaked at 6 m s^{-1}. A smaller updraft was located northwest of the main updraft. Updrafts measured during passes 6 and 7 were weak. No significant downdrafts were measured on any of the three passes. The measured peak liquid water content in pass 5 was 1 g m^{-3}. Again, there was reasonably good correspondence between the shape and location of the vertical motion and liquid water fields. Liquid water contents measured during passes 6 and 7 were less than 0.4 g m^{-3}.

Raindrops with diameters >1 mm were present throughout pass 5. Large (2–4 mm) and giant (>4 mm)

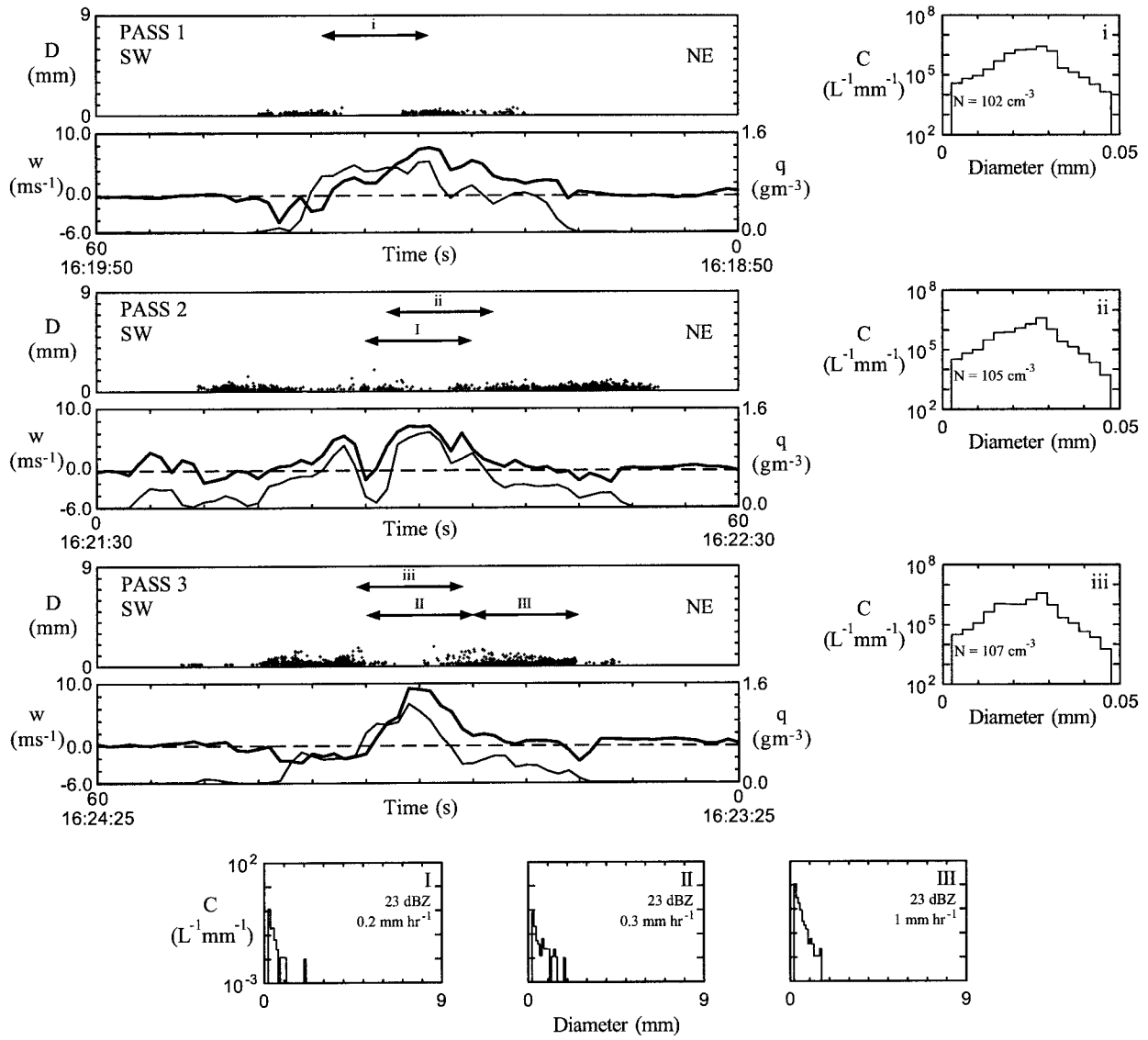

FIG. 4a. Aircraft measurements of thermodynamic and microphysical parameters during cloud passes 1–3 on 23 July 1985. The top panel for each pass illustrates the size of each drop measured by the 2D-P probe during the pass as a function of time (distance along the flight path). The bottom panel shows the updraft velocity and JW measurement of cloud liquid water. FSSP cloud droplet spectra are shown to the right of the panels, and 2D-P raindrop spectra are shown on the bottom of the figure. These spectra were averaged over regions indicated by arrows on the top pass of each of the panels. Calculated reflectivities and rainfall rates are shown for each of the raindrop spectra.

raindrops, including a 6.4-mm drop, were found within the strongest updraft. On pass 6, a region approximately 1.5 km wide contained raindrops larger than 3 mm. Several raindrops with diameters as large as 5 mm were observed on the northwest side of the updraft. Note that small raindrops ($D < 1$ mm) were absent from the region where the largest raindrops were observed and only a few 1–2-mm raindrops were sampled. On pass 7, the large raindrops (2–4 mm) were sampled over a 2.5-km region, and the giant raindrops were confined to a 0.3-km region. The largest raindrop observed was 8.2 mm. The reflectivities calculated from the drop spectra averaged over a distance of approximately 1 km along the flight track in the giant-raindrop regions (VII, VIII, and X) of passes 5, 6, and 7 were 51, 54, and 58 dBZ, with rainfall rates of 16, 40, 47 mm h^{-1}, respectively. Calculated reflectivities in the large raindrop regions (VI, IX, and XI), but outside the regions containing the giant raindrops, ranged from 36 to 47 dBZ. These data show the importance of giant raindrops to the development of extremely high reflectivity in the Hawaiian rainband clouds.

Passes 8 and 9 were made well below cloud base at 150 m. Vertical motions were weak at this level. Drops with diameters up to 2 mm were common throughout the pass. An ~1.4 km wide region on each pass con-

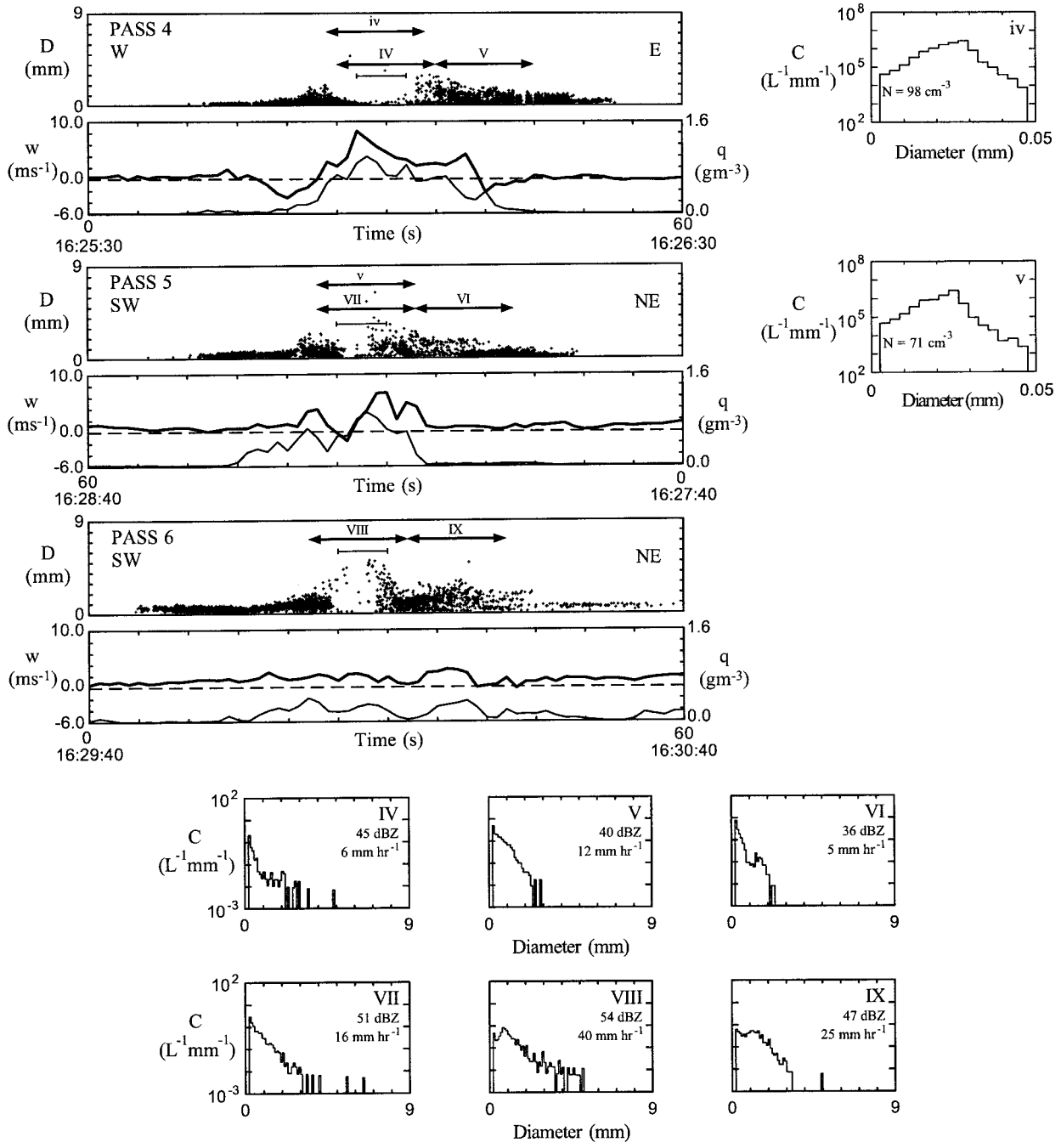

FIG. 4b. Same as 4a except for passes 4–6 on 23 July 1985. The horizontal bars with vertical end caps denote the location of the 5-s drop spectra used in the breakup calculations.

tained drops with diameters >2 mm. Very few drops had diameters exceeding 3 mm.

For reasons discussed in section 2, we will relate these data to the evolution of high reflectivity cores observed with Doppler radars during HaRP. We chose 10 August 1990 because the thermodynamic sounding for that day (Fig. 2b) was very similar to the 23 July 1985 sounding (Fig. 2a), and the entire life cycles of two high reflectivity cores were observed by the radars (Part I). Table 1 shows a detailed comparison of the offshore environment during the morning hours of 23 July 1985 and 10 August 1990. The clouds (Figs. 4 and 5) were sampled at approximately the same time of day and the same distance offshore. The LCL and the EL for air parcels originating in the surface mixed layer were very similar, and the clouds were of similar depth. Comparable CAPE

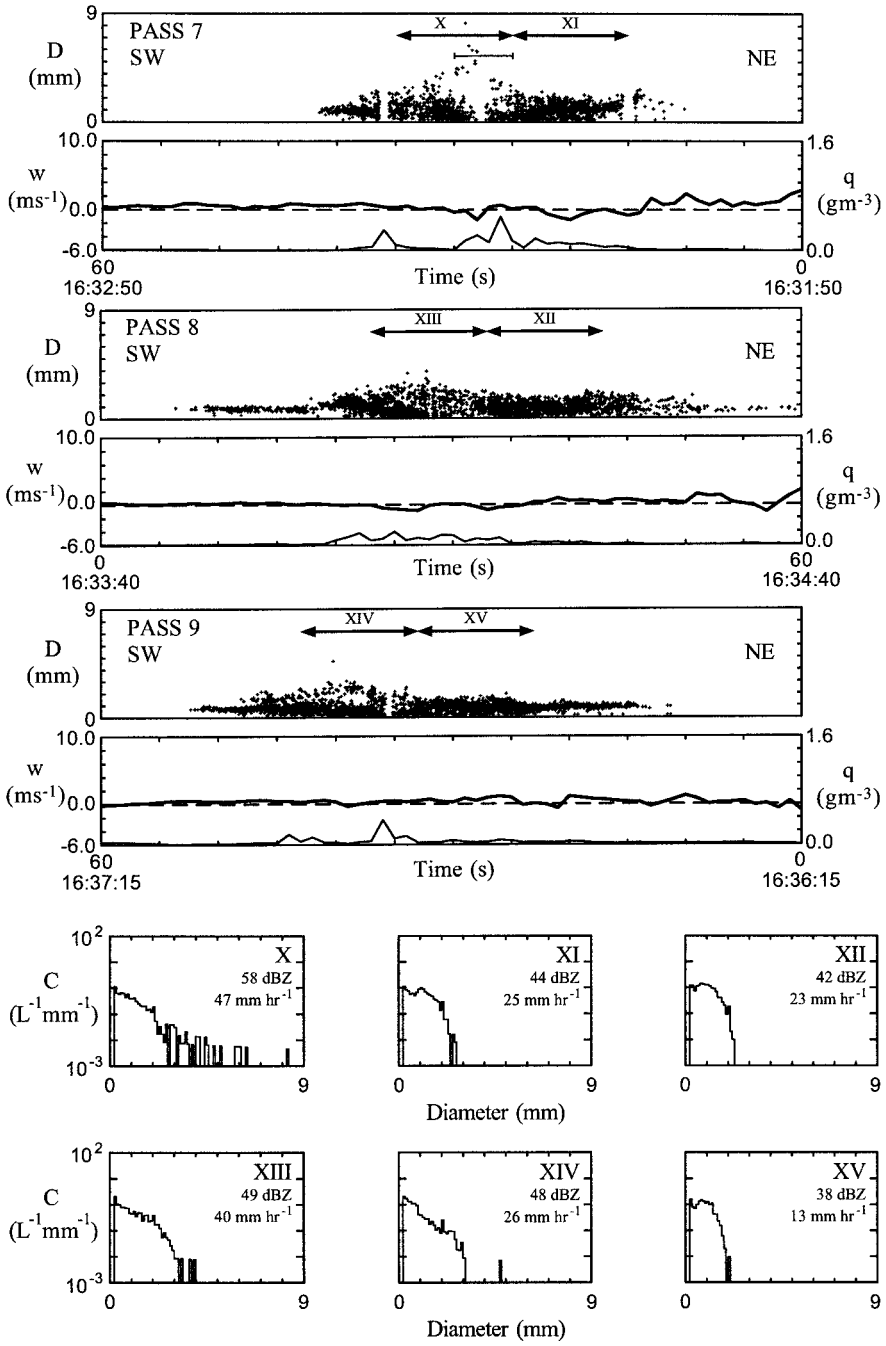

FIG. 4c. Same as 4a except for passes 7–9 on 23 July 1985. The horizontal bars with vertical end caps denote the location of the 5-s drop spectra used in the breakup calculations. FSSP data are not included for low-level passes.

values suggest that the peak updrafts should have been within 2 m s^{-1} of each other. The vertical profiles of adiabatic liquid water content, based on a simple 1D parcel ascent model, were almost identical since the cloud-base mixing ratios and temperatures were almost the same. Northeasterly winds were between 2 and 5.5 m s^{-1} in the trade wind layer, and no strong vertical shear was present, suggesting that the updrafts in both cases were nearly vertical, and that the general speed and direction of the cells' movement were the same.

Radar data indicate that the lifetimes of the high reflectivity cores on 10 August were about 10–15 min. The aircraft observations on 23 July shown in Fig. 4 were obtained over an 18-min period. The data in passes 1–4 on 23 July appear to have been collected prior to the development of a high reflectivity core. If one as-

TABLE 1. Sounding comparison for 23 July 1985 (Fig. 2a) and 10 August 1990 (Fig. 2b).

Parameter	23 July 1985	10 August 1990
Inversion base height	2350 m (765 mb)	2300 m (770 mb)
Winds in the trade wind layer	NE at 2–5 m s^{-1}	ENE at 3.5–5.5 m s^{-1}
LCL	750 m (925 mb)	630 m (940 mb)
LFC	995 m (900 mb)	720 m (940 mb)
EL	2420 m (755 mb)	2410 m (755 mb)
CAPE	52 J kg^{-1}	76 J kg^{-1}
Maximum updraft based on CAPE	10.2 m s^{-1}	12.3 m s^{-1}
Estimated cloud depth	2200 m	2350 m
Cloud-base temperature	17.5°C	18.5°C
Cloud-top temperature	10.5°C	9.5°C
Surface temperature and moisture	22.5°C	23.5°C
Surface mixed layer mixing ratio	12.8 g kg^{-1}	14 g kg^{-1}
Adiabatic cloud liquid water at EL	3.75 g kg^{-1}	3.85 g kg^{-1}

sumes that the 23 July and 10 August clouds had similar temporal evolution, the early radar structure on 23 July should have corresponded to the 10 August radar structure shown in panels A1–C1 and A2–D2. The reflectivities calculated from the raindrop spectra during passes 5–7 suggest that the sampling during these passes occurred during the most intense stage in the evolution of the 23 July high reflectivity core. The highest calculated reflectivity (58 dB*Z*) occurred in region X of pass 7 at 400 m. This stage of the 23 July core corresponds to the 10 August high reflectivity cores in panels E1 and F2/G2 of Fig. 5. The calculated reflectivities from the aircraft data are subject to uncertainty because of poor sampling statistics associated with the giant raindrops. Nevertheless, the calculated reflectivities shown in passes 5–7 agree very well with the peak reflectivity values observed with the radars (e.g., Fig. 5). Passes 8 and 9 and subsequent passes on 23 July were during the dissipation stage since calculated reflectivities were slowly decreasing with time and were less than 50 dB*Z*. These passes correspond to the 10 August cell shown in panels F1 and G1.

The stronger updraft areas (>4 m s^{-1}) in passes 1–4 were capable of supporting 1-mm raindrops. The peak updraft speeds for this case were close to the maximum possible value estimated from the CAPE, implying that the core of the updraft was nearly adiabatic. The strongest updraft, which exceeded 9 m s^{-1} (pass 3, Fig 4a), was capable of supporting raindrops as large as 5 mm. Although the structure of the liquid water content field mirrored the structure of the vertical velocity, particularly in passes 2–4 of Figs. 4a and 4b, the maximum measured liquid water contents were approximately half of their adiabatic value. According to earlier studies, the JW probe underestimates the mass of large ($\sim D > 30$ μm) cloud droplets (Owens 1957; Knollenberg 1972; Baumgardner 1983). Personne et al. (1982) showed, in some cases, that the underestimate of cloud liquid water may be as large as 50% when significant concentrations of large cloud droplets are present. Large cloud droplets were common in the maritime clouds sampled in this study (e.g., cloud droplet spectra in regions i–v). These calibration studies, together with measurements of updraft speeds near the maximum value based on the CAPE, suggest that the core of the updraft remained nearly unmixed and that the true liquid water content was close to adiabatic.

Raindrops were generally observed in low concentrations in the peak updraft regions during the early passes. This absence of large raindrops in the peak updraft regions in passes 1–3, the first observation of two large raindrops in pass 4, and subsequent appearance of large raindrops at lower altitudes below the updraft core in passes 5–7 together suggest that initially the larger raindrops were suspended in the updraft above the flight level. At the time of the later passes, raindrops originally supported by the main updraft were large enough to fall through the flight level against the weakening updraft. During the descent they grew further by accretion of cloud water within the updraft region. This explanation, supported by calculations presented in section 4, is generally consistent with the evolution of the reflectivity and vertical velocity fields associated with radar-observed high reflectivity cores reported in Part I.

An ''anvil-like'' overhang was commonly observed on the flanks of updrafts in the HaRP data as the vertical flow decelerated and diverged at the inversion (see Part I). During this time, the reflectivity pattern indicated that smaller precipitation drops were transported horizontally out of the updraft near cloud top. The radar reflectivity pattern showed the overhang deepening downward with time, indicating that raindrops within the overhang were falling toward the surface. Weak downdrafts were sometimes resolved in the upper part of the overhang. The region of smaller raindrops on both sides of the updraft in passes 1–5 shows the microphysical structure of the overhang region. The overhang region contained little cloud liquid water. The size of the raindrops within the overhang region decreased away from the main updraft, consistent with the reflectivity data in Fig. 5 and other cases presented in Part I. The smaller raindrops, because of their low terminal velocities, were carried farther away from the updraft within the outflow near the inversion.

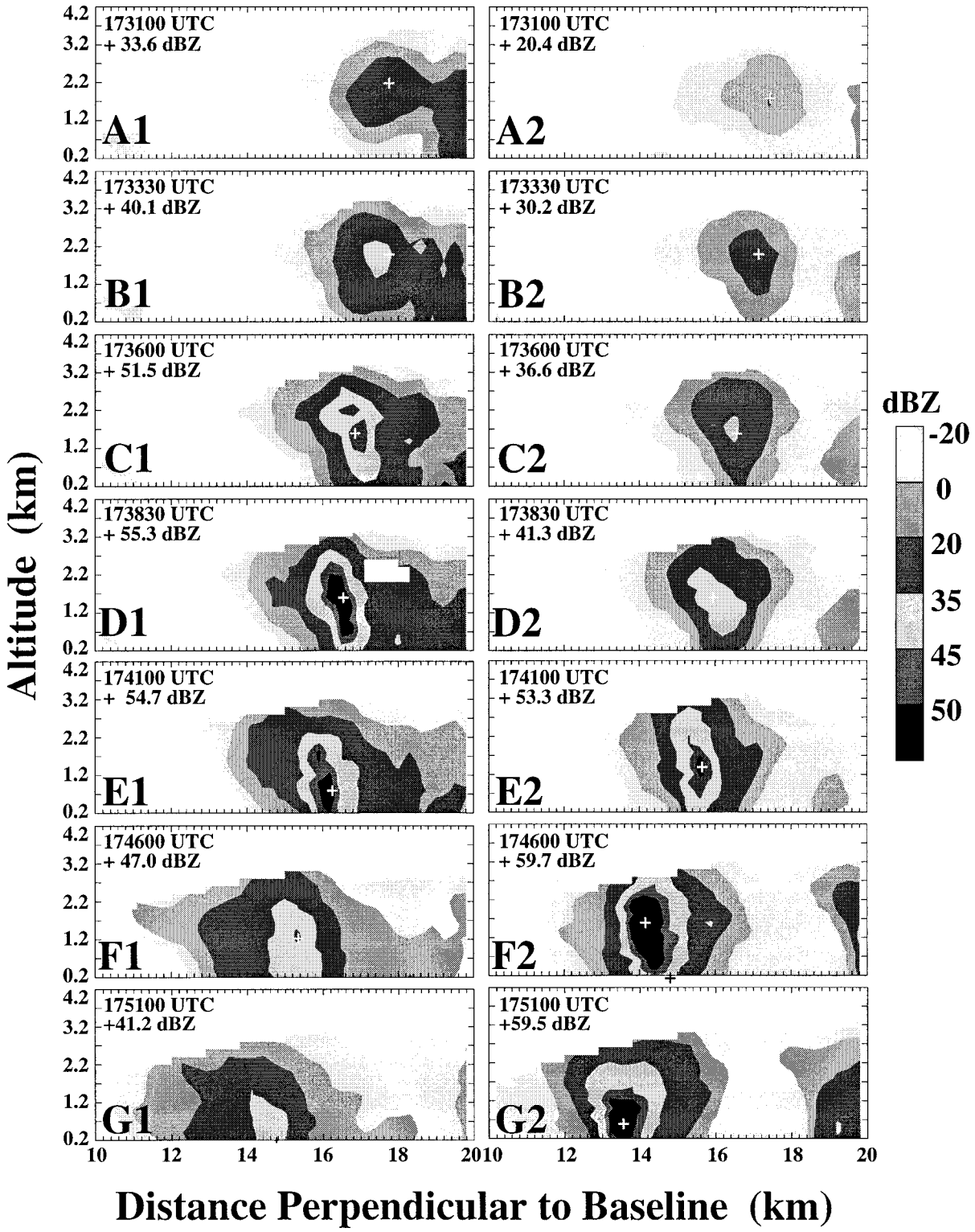

FIG. 5. Evolution of two high reflectivity cores embedded in a rainband on 10 August 1990. (a1)–(g1) Vertical cross sections of the CP3 radar reflectivity field between 1731 and 1751 UTC through a life cycle of a rain shaft (core 1). (a2)–(g2) Same as (a1)–(g1) but for another high reflectivity core approximately 1.5 km northwest of core 1.

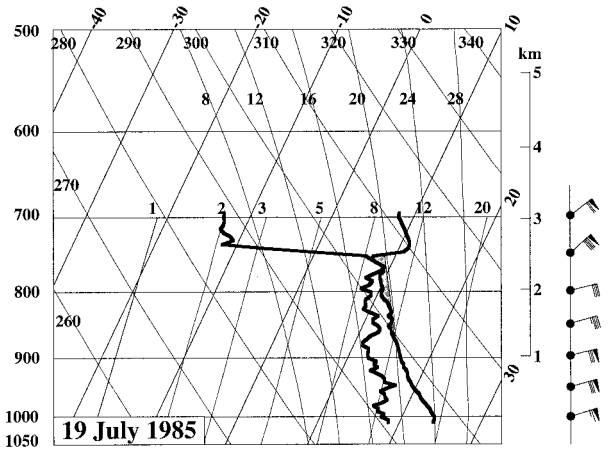

FIG. 6. Thermodynamic sounding on 19 July 1985 at approximately 1610 UTC. Conventions are the same as for Fig. 2a.

b. 19 July 1985

The 19 July 1985 rainband contained a vigorous cell that extended into the inversion layer. Large raindrops (>2 mm) were found suspended near the cell's summit. Giant raindrops eventually appeared in the lower part of the cloud as drops initially suspended near the cloud top grew and fell. Penetrations were made along the rainband, so the reflectivity overhang, which is most prominent in the cross-band direction, was not as apparent. This case, a second example of the development of a high reflectivity core within a cell with a vigorous updraft, provides insight into the variations in raindrop size distribution that occur along the rainbands within and outside high reflectivity cores.

The environment on 19 July 1985 (Fig. 6) was characterized by a mixed layer between the surface and 580 m, an LCL at 890 m, and an LFC at 1260 m. The trade wind layer was conditionally unstable with a CAPE of 49 J kg^{-1}, corresponding to a maximum possible adiabatic updraft of 9.9 m s^{-1}. A 3.9°C inversion was located between 2410 m and 2575 m. The trade winds below the inversion in the cloud layer were generally east-northeasterly with speeds ranging from 4 to 8 m s^{-1}.

The King Air flew along a rainband located over land northwest of Cape Kumukahi. Figure 7, the horizontal and vertical flight track between 1649:00 and 1707:30 UTC, shows the location and elevations of the cloud passes. The King Air penetrated a cell containing a high reflectivity core during an 18-min period of passes along the rainband. Data collected in seven cloud passes between 1618:50 and 1637:15 UTC are shown in Figs. 8a and 8b. The panels are aligned so that the cell containing the largest raindrops is positioned near the center of the pass, and the south end of the pass is on the left side of each panel. Figure 8 also shows the cloud droplet and raindrop spectra for selected cloud regions, denoted by the horizontal arrows. The cloud droplet spectra were averaged over distances ranging from 0.5 to 1 km (regions i–vi). The raindrop spectra were averaged over 1 km (regions I–XIII).

The King Air penetrated the top of a vigorous convective cell that extended into the inversion layer during passes 1 and 2 at 2.9 km (Fig. 8a). Downdrafts on the flanks of the narrow cloud turret in pass 1, and the low observed liquid water content of 0.8 g m^{-3}, indicate that evaporative cooling and mixing occurred at the cloud top as the cloud grew through the flight level. Drizzle drops with diameters between 0.1 and 0.7 mm were found at the top of the growing cloud turret. The cloud droplet concentration was low in region i (107 cm^{-3}) relative to later cloud passes in regions ii–vi (150–250 cm^{-3}) with a modal diameter of 25 μm. Two minutes later, during the second pass, large raindrops (2–2.5 mm) were found near the cloud top. The peak updraft velocity of 7 m s^{-1} was capable of supporting a drop as large as 2.2 mm. The larger raindrops (>1.5 mm) observed in the cell were either suspended or rising near the updraft core but were falling on its flanks. The reflectivity, calculated from the raindrop spectra (region I, Fig. 8a), was 36 dB*Z*. Downdrafts of 1–2 m s^{-1} were again present on the sides of the updraft, associated with evaporation on the flanks of the cell. The largest drops were embedded in a cloud with an average measured liquid water content of 1.5 g m^{-3} and cloud droplet concentration of 156 cm^{-3} (region ii).

A broader updraft was observed at 2500 m during pass 3. Other weaker, narrow updrafts were present along the rainband (Fig. 8a). Downdrafts with peak velocities between 4 and 6 m s^{-1} and horizontal scales smaller than the main updraft were present on the sides of the updrafts. Large raindrops with diameters between 2.0 and 3.0 mm were found within a region approximately 2 km wide in the southern portion of the main updraft. The calculated reflectivity in region II was 42 dB*Z*. The larger raindrops were located in a cloud that had a measured liquid water content ranging from 0.6 to 1.2 g m^{-3}. Smaller raindrops (<1 mm) were common in other updraft regions, while in other parts of the band raindrop diameters were typically <0.5 mm.

The updraft on pass 4 at 2000 m was composed of four turrets (Fig. 8a), three adjacent, and a fourth 700 m to the south of the three. The measured liquid water content in the region across the four turrets ranged from 0.4 to 1.3 g m^{-3}. Raindrops as large as 2 mm were observed across the entire updraft region. The largest raindrops (2–4 mm) were found on the northern edge of the southernmost turret (region V) where the calculated reflectivity was 45 dB*Z* and the peak updraft was 4 m s^{-1}. The change in raindrop spectra between the updraft and the surrounding rainband resulted in a calculated horizontal reflectivity gradient of 26 dB*Z* over ~2 km (regions III–V, Fig. 8a). The highest updraft speed of 7 m s^{-1} was recorded in the northernmost turret where no drops larger than 2 mm were sampled; however, the measured cloud liquid water and cloud drop

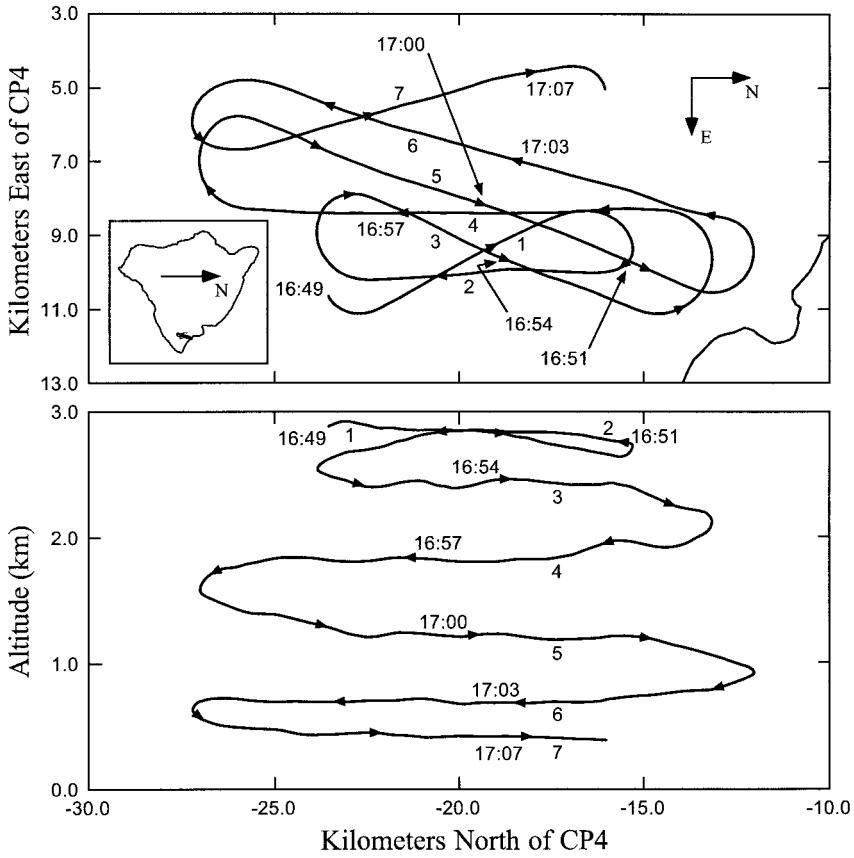

FIG. 7. UW King Air horizontal (top) and vertical (bottom) flight track on 19 July 1985 between 1649 and 1707 UTC.

concentration were highest at 1.3 g m^{-3} and 247 cm^{-3}. Small raindrops ($D < 1$ mm) were present along the entire rainband.

Pass 5 was made in the lower part of the cloud at 1.2 km. A region of very large raindrops (2–6.5 mm) was encountered on both passes. On pass 5, the large drop region was approximately 4 km wide, centered on the main updraft core. The giant raindrops were embedded in a narrow 200-m region of a 6 m s^{-1} updraft. This double-peak updraft, sampled only 300 m above the LCL and near the LFC (based on the upstream sounding), was exceptionally strong. The location of the rainband is consistent with the position of the low-level convergence associated with the island-induced flow reversal (Smolarkiewicz et al. 1988; Rasmussen et al. 1989) and the observed updraft was likely enhanced by low-level convergence. The measured peak liquid water content was approximately adiabatic, based on the 890-m LCL estimated from the offshore sounding. The calculated reflectivity in region VII (Fig. 8b), which contained the largest raindrops, was 53 dBZ, while the 4-km-wide large raindrop region outside of the high reflectivity core had a reflectivity of about 45 dBZ (regions VI, VII, and IX).

Pass 6 was made just above cloud base. The cloud droplet spectrum (region vi) had a mode of 10 μm, but cloud droplets as large as 45 μm were sampled. Updrafts at this level were weak, but the giant drop region sampled on the previous pass was still present approximately underneath the strong updraft core. Raindrops in the surrounding 3–4 km were generally smaller than 2 mm. The calculated reflectivity within the large raindrop region (XI) was 54 dBZ, while 3 km south in region X, the reflectivity was 28 dBZ. The corresponding rainfall rates were 37 and 2 mm h^{-1}. The final pass, pass 7, was made below cloud base at 500 m. Giant raindrops were not observed during this pass. The calculated reflectivity in the region of heaviest precipitation was approximately 44 dBZ (region XII).

The 19 July case was the only case where a strong cell was penetrated very close to its top during its developing stage. The data from pass 2 not only demonstrates that large (>2 mm) raindrops can exist near cloud top during the developing stage of a high reflectivity core but also that the magnitude of the updrafts near cloud top are sufficient to either suspend these drops or carry them upward.

The rapid growth of raindrops in the upper part of the cloud is consistent with high values of reflectivity observed during HaRP. Typically high reflectivity cores

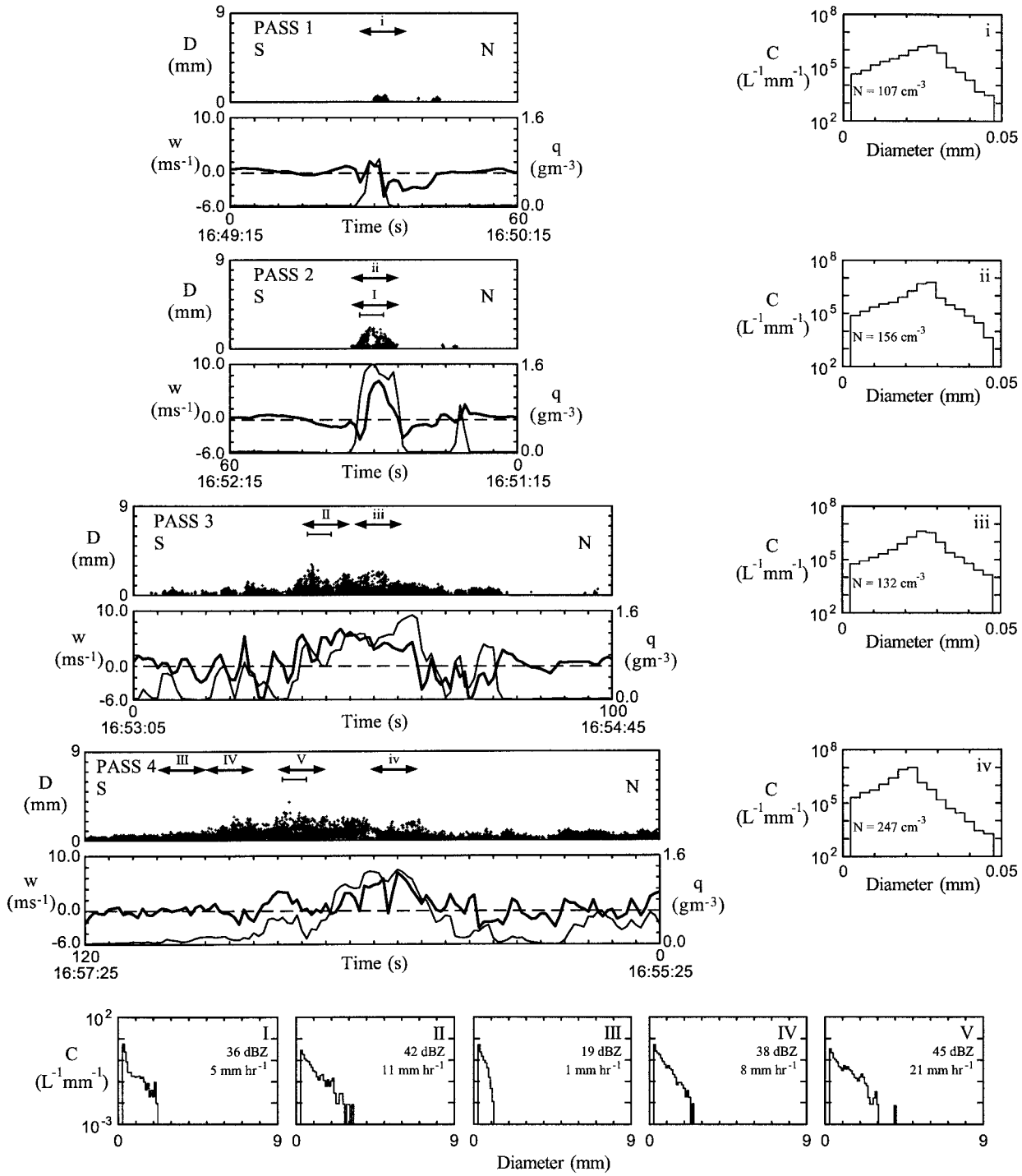

FIG. 8a. Same as Fig. 4a except for passes 1–4 on 19 July 1985. The horizontal bars with vertical end caps denote the location of the 5-s drop spectra used in the breakup calculations.

first appeared in the middle part of cells (between the levels of passes 4 and 5) as raindrops grew to large sizes while falling through the updraft (e.g., Fig. 5). In some cases, such as the 22 August 1990 cell shown in Fig. 9, the peak reflectivity (60.5 dBZ) formed within 600 m of the cloud top and the 50 dBZ contour extended to near the cloud-top level. In cases such as 22 August, the larger raindrops must have remained suspended near cloud top within the updraft for most of their growth (the updraft in the cloud-top region must have main-

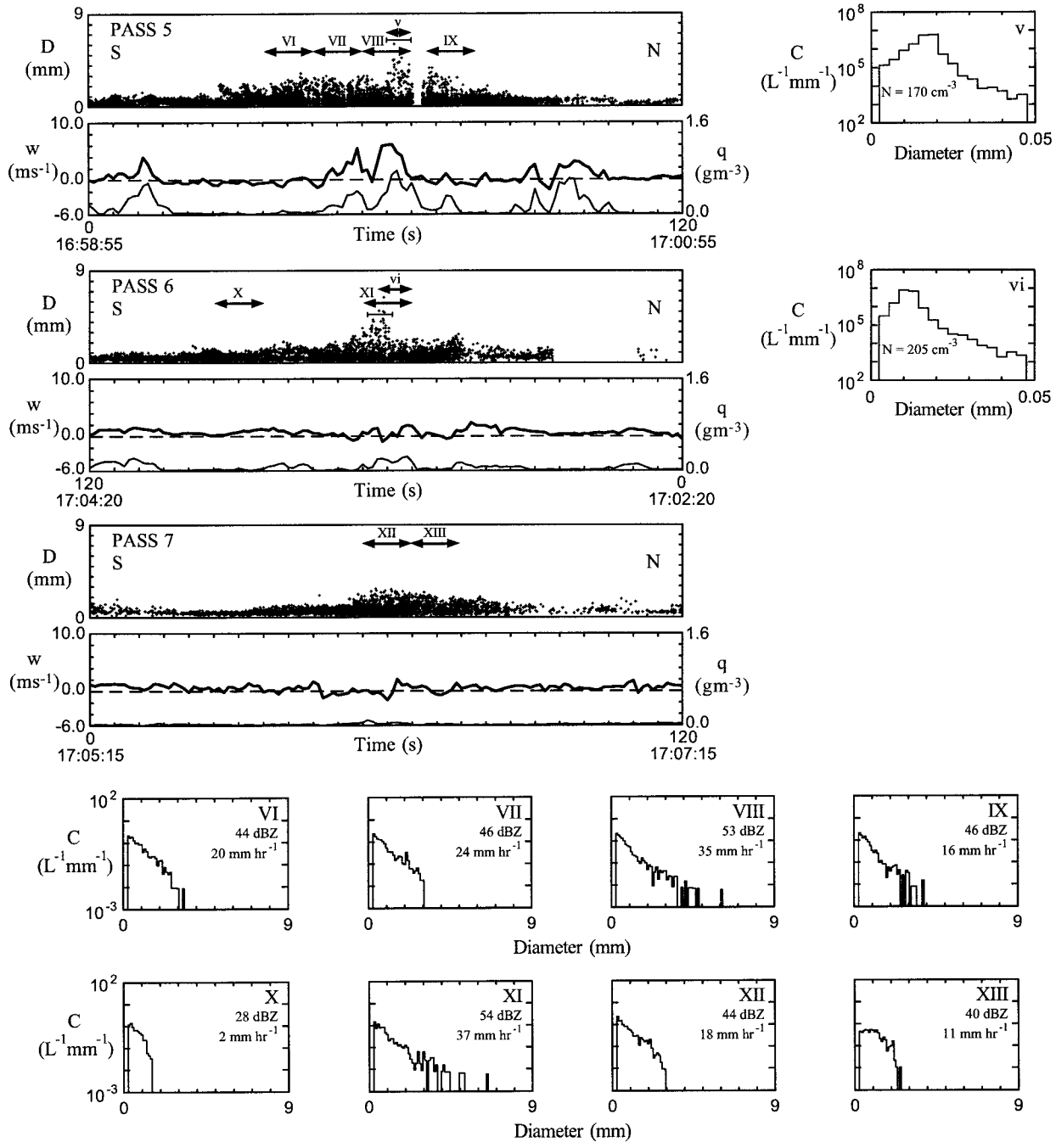

FIG. 8b. Same as Fig. 4a except for passes 5–7 on 19 July 1985. The horizontal bars with vertical end caps denote the location of the 5-s drop spectra used in the breakup calculations. The gap in pass 5 is a region of missing data.

tained an intensity of 8–10 m s^{-1} during the growth period).

In the aircraft data, giant raindrops ($D > 4$ mm) typically occupied a narrow part of the cloud (~200 to 500 m wide) and were surrounded by regions of precipitation characterized by smaller raindrops and lower calculated reflectivities. The variations in the alongband structure observed on 19 July can be interpreted in the context of overall rainband structure by comparing the aircraft data to alongband reflectivity and vertical velocity cross sections from 22 July 1990 during HaRP (Fig. 10). Three rain shafts, two mature and one developing, appear in Fig. 10. The dimensions and magnitude of the high reflectivity cores are qualitatively consistent with the reflectivity calculations based on the 19 July aircraft data, if one accounts for the averaging associated with

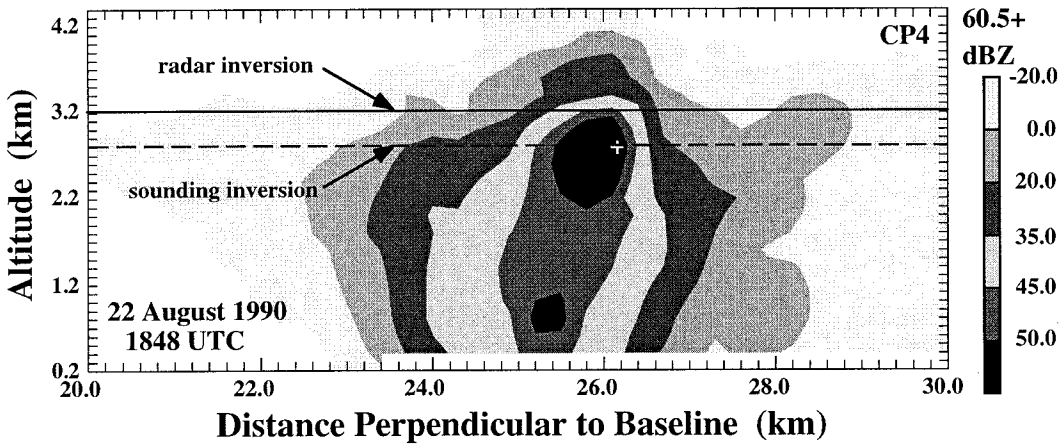

FIG. 9. Vertical cross section of radar reflectivity through a cell at 1848 UTC on 22 August 1990. Two estimates of the trade wind inversion are shown, the first based on the sounding and the second based on the top of the weak echo region outside the main reflectivity core. The extension of the echo to altitudes above 3.6 km over the high reflectivity region in Fig. 8 is due to sidelobe contamination (see Part I).

the sampling and interpolation of the radar data. The reflectivity gradients between the intense rain shaft and the surrounding rainband are also consistent with the calculated reflectivity gradients from the raindrop spectra. The maximum reflectivity was located in the middle to upper part of the cloud in the developing rain shaft on the left side of Fig. 10. As suggested by the aircraft data from 19 July, this time period in the life cycle of the rain shaft corresponds to the time when raindrops, initially suspended near the top of the cloud, grow rapidly as they start falling through the updraft toward cloud base.

4. Discussion

a. Microphysical structure and raindrop growth within high reflectivity cores

The microphysical and kinematic measurements from JHWRP were generally consistent with the radar analyses of the structure of rainbands containing high reflectivity cores determined from the HaRP radar data. Reflectivities calculated from drop size distributions in the central rain shafts ranged from 52 to 58 dB*Z*, in good agreement with values observed in the high reflectivity cores discussed in Part I. Calculated reflectivities in excess of ~50 dBZ and corresponding rainfall rates as high as 47 mm h^{-1} were always associated with the presence of giant raindrops. In the radar analyses, the highest reflectivities developed in the strongest updrafts, taking into account the time lag required for raindrop growth (see Part I). The aircraft analyses showed that the giant raindrops formed in the regions of the strongest updrafts. Calculated reflectivities in regions adjacent to the main rain shafts, where giant raindrops were not present, were generally in the range of 35–45 dB*Z*. Raindrops falling from the ''anvil'' outflow region (23 July) and between strong rain shafts (19 July) had calculated reflectivities in the range of 15–30 dB*Z*. Ra-

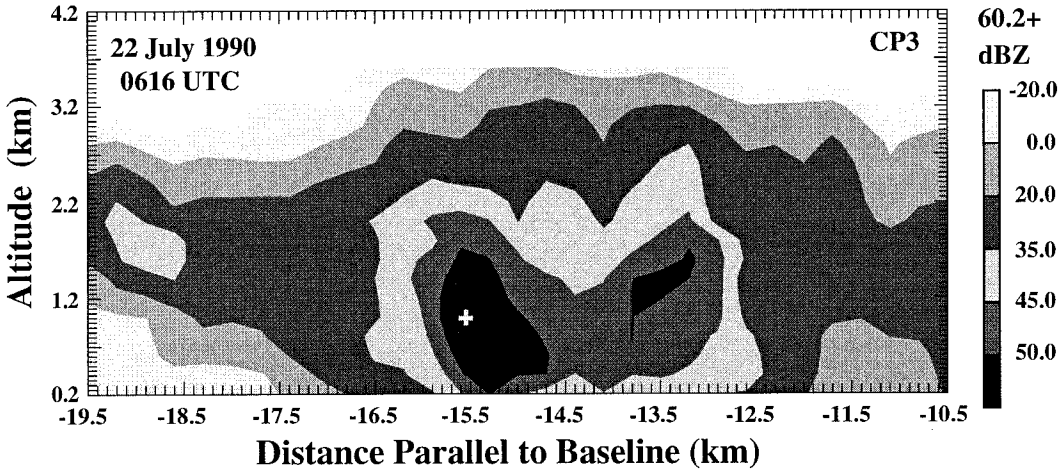

FIG. 10. Vertical cross section of radar reflectivity along a rainband at 0616 UTC 22 July 1990.

dar analyses (e.g., Fig. 5) showed that after the initial formation of the anvil, the reflectivity overhang descended to the surface leading to an overall widening of the rainband. The absence of cloud water under the anvil regions sampled by the aircraft during JHWRP suggest that any growth of raindrops in these regions would have been limited to self collection.

In both the radar and the aircraft data, downdrafts >2.5 m s^{-1} were only found in the upper parts of rainbands and were likely associated with evaporative cooling as the cloud tops penetrated into the very dry air above the trade wind inversion. Downdrafts were not observed (aircraft) nor synthesized (radar) in the lower part of the clouds. The aircraft data indicated that the updrafts and downdrafts in the upper parts of the cloud had smaller scale structure (i.e., pass 3, Fig. 8a) than could be resolved with the radar syntheses.

An important uncertainty related to the evolution of precipitation in these clouds was the degree to which the cloud liquid water content in the updraft was undiluted. The measured peak liquid water contents within the main updrafts in the lower part of the clouds were near adiabatic, but in the middle and upper parts of the cloud the peak liquid water contents were half, or less, of their adiabatic values. The incomplete response of the JW instrument to larger cloud droplets may partially account for this observation since the droplet spectra are broader in the upper part of the clouds. The peak updrafts were near the maximum value calculated from offshore sounding CAPE. If buoyancy were the dominant forcing of the updraft, then this would imply that the cores of the updrafts were nearly adiabatic. The rainbands were sampled near the location of the flow separation line discussed by Smolarkiewicz et al. (1988) and Rasmussen et al. (1989). Although it is unclear how much of the magnitude of the updrafts observed on the two days was due to forcing from convergence along this line, estimates from recent model simulations (Grubisic et al. 1996, personal communication) suggest that the contribution is no more than 0.5 m s^{-1}. The strength of the updrafts, particularly near cloud top, together with the known underestimate of liquid water content by the JW probe in clouds containing large cloud droplets (e.g., Personne et al. 1982), suggest that the actual liquid water content was much closer to the adiabatic value within the cores of the updrafts than the liquid water content measurements would indicate.

The close correspondence between the shape and location of high reflectivity cores and their parent updrafts (Part I) led us to infer that raindrops first developed within the strongest updrafts near cloud top several minutes prior to the observation of the highest reflectivities. This finding is consistent with earlier observations of shallow cumulus clouds over the Caribbean by Saunders (1965). During this early period of raindrop growth, cells must maintain updrafts with speeds greater than the terminal velocities of the raindrops to suspend, or carry them upward. The radar data implied that large raindrop formation continued throughout the middle and upper part of the clouds for a period of several minutes after updrafts reached their peak intensities. The data further suggested that as the raindrops fall against the weakening updrafts, they rapidly grow to sizes sufficient to produce the high reflectivities in the middle part of the cloud.

The 19 July case demonstrated that growing raindrops with diameters of 1–2 mm were present near the top of rising cloud turrets in updrafts that were strong enough to suspend them. Calculations using a simple one-dimensional collection model (Rogers and Yau 1989, 131) with updraft and cloud liquid water content values changing with altitude according to the 19 July aircraft observations indicate that the 1–2 mm drops observed at cloud top would double their size during the near-suspension period of 2–3 min. Our calculations showed that these drops could grow to 4–6 mm through accretion of cloud water alone in less than 10 min during their suspension and subsequent fall through the cloud, provided they remained within the region of strongest updraft and in high liquid water content during their fall. Raindrops as large as 4–6 mm were sampled low in the cloud during passes 5 and 6, approximately 8.5 min after the 1–2 mm drops were observed at cloud top.

The sensitivity of our calculations to the value of the cloud liquid water content was tested by assuming that the 2-mm raindrops observed on pass 2 at 2.85 km grew while falling at a mean terminal velocity of $\sim$8 m s^{-1} through a mean $\sim$5 m s^{-1} updraft. Assuming a collection efficiency of unity and half-adiabatic liquid water content, the drops arrived at 1.25 km (the elevation of pass 5) in about 8 minutes and grow to approximately 5.6 mm. When we prescribed an adiabatic liquid water content profile, the 2-mm drops originally suspended near cloud top grew to sizes greater than 8 mm (the largest drop sampled on 23 July was 8.3 mm) in less than 8.5 minutes. These simple calculations suggest that the high reflectivity cores can develop as a result of simple accretional growth, provided that the raindrops remain in the updraft. These findings support the earlier study of Saunders (1965), who attributed rapid intensification of radar reflectivity in shallow cumuli to growth by gravitational coalescence.

The absence of significant vertical wind shear is critical for growing raindrops to remain in the updrafts during their full up–down trajectories. Shear produces tilted updrafts so that raindrops falling from cloud top cannot remain suspended in the updraft and are deprived of the high liquid water content environment during a large part of their fall. As demonstrated in the soundings in Figs. 2 and 4 and in Part I, and in Doppler syntheses of the kinematic structure of high reflectivity cores (Part I), shear in the trade wind environment upwind of Hawaii is often weak through most of the depth of the trade wind layer. As a result, updrafts in many cases are nearly vertical, and growing raindrops within the updraft

core can remain in high liquid water regions throughout their growth and fall to the surface.

b. Importance of raindrop breakup

Raindrops undergo breakup by colliding with other raindrops or by growing to such large sizes that they become hydrodynamically unstable. In the case of hydrodynamic instability, the formula of Komabayasi et al. (1964) predicts mean drop lifetimes of several minutes for $D = 5.5$ mm to less than one minute for $D > 7$ mm. Pruppacher and Klett (1997, 413) give reasons why Komabayasi's results do not typically apply to atmospheric processes. Wind tunnel measurements by Pruppacher and Pitter (1971) have shown that the largest drops that are stable in quiescent air have equivalent spherical diameters of approximately 9 mm. Since all of the drops observed in the Hawaiian clouds were smaller than this size, we limit our discussion to collisional breakup. Historically, model and laboratory results have supported the view that collisional breakup should rapidly destroy larger drops in natural clouds and limit drop diameters to a maximum of about 2–3 mm (List and Gillespie 1976; Gillespie and List 1978; Takahashi 1978; Low and List 1982). An appropriate estimate of collisional breakup (Beard et al. 1986) is found by calculating the collision rate (Q) of a large drop (D) with all smaller drops (d) using a measured drop spectrum $C(d)$:

$$Q(D, d, C) = \left(\frac{\pi}{4}\right) \sum_{d_0}^{d_f} [(D + d)^2 (V_T - v_T) C(d)],$$

where V_T and v_T are the terminal velocities of the large and small drops. The range of smaller drops (d_0 to d_f) that produce breakup is limited to inelastic (coalescing) collisions where the excess kinetic energy exceeds one-half the surface energy of the large drop (Beard et al. 1983). A further reduction of this collision rate by 80% is needed to account for the laboratory observation that only the most direct (20%) of collisions cause the large drop to disintegrate (McTaggart-Cowan and List 1975). Thus, the formula for calculating the breakup collision rate is

$$Q'(D, d, C) = 0.05\pi \sum_{d_0}^{d_f} [(D + d)^2 (V_T - v_T) C(d)].$$

The inverse of this breakup collision rate is the mean time between breakup events:

$$t_b(D, d, C) = \frac{1}{Q'}.$$

Because of the random spatial distribution of the small drops we use the Poisson distribution formula $P(n, k) = n^k e^{-n}/k!$ (Feller 1957) to represent the probability of a large drop encountering k drops (k breakup events) over a fall interval where collisions with n drops (n breakup events) are expected. The probability of no breakup collisions ($k = 0$) in the interval where n breakup events are expected is given by

$$P(n, 0) = e^{-n}.$$

Since we are interested in the breakup probability of the largest drops during the interval when they fall through a rainshaft, we calculate the number of expected breakup events given by the ratio of the fall time (t_f) to the mean time to breakup (t_b): $n = t_f/t_b$. For a fall time much shorter than the expected time to breakup, where $n \ll 1$, the probability that no breakup collisions occur is $P(n \ll 1, 0) = 1 - n$. This "survival" probability approaches 1 as n approaches zero. For a fall time much longer than the expected time to breakup ($n \gg 1$), the probability that no breakup collisions occur approaches zero exponentially as n increases linearly (see previous equation).

Sections a–c of Table 2 show the calculated survival probabilities ($P = e^{-n}$) of large drops encountering no breakup events ($k = 0$) during a fall time t_f having n expected breakup events, where $n = t_f/t_b$, calculated for a selected range of initial raindrop sizes. The calcula-

TABLE 2. Survival probabilities for raindrops observed: (a) 23 July 1985 (10-s spectra), (b) 23 July 1985 (5-s spectra), (c) 19 July 1985 (10-s spectra).

	Drop size (mm) *and survival probabilities P* (%)			
(a)				
Layer 1 (1750–1350 m)	**3**	**4**	**5**	**6**
(spectrum from region IV)	*84.2*	*83.5*	*81.0*	*91.4*
Layer 2 (1350–800 m)	**4.2**	**5.1**	**6.1**	**7.1**
(spectrum from region VII)	*37.5*	*31.0*	*30.1*	*29.6*
Layer 3 (800–400 m)	**4.6**	**5.5**	**6.5**	**7.5**
(spectrum from region VIII)	*52.5*	*47.8*	*50.7*	*51.5*
Final drop size	**4.6**	**5.6**	**6.6**	**7.6**
P (joint)	*16.7*	*12.4*	*12.4*	*12.8*
P' (joint)	*40.8*	*35.2*	*35.2*	*35.5*
(b)				
Layer 1 (1750–1350 m)	**3**	**4**	**5**	**6**
(spectrum within region IV)	*98.5*	*98.2*	*97.3*	*98.9*
Layer 2 (1350–800 m)	**4.2**	**5.1**	**6.1**	**7.1**
(spectrum within region VII)	*70.5*	*63.2*	*55.8*	*50.1*
Layer 3 (800–400 m)	**4.6**	**5.5**	**6.5**	**7.5**
(spectrum within region VIII)	*91.3*	*89.8*	*89.0*	*88.5*
Final drop size	**4.6**	**5.6**	**6.6**	**7.6**
P (joint)	*63.4*	*55.7*	*48.3*	*43.9*
P' (joint)	*79.8*	*74.8*	*69.5*	*66.3*
(c)				
Layer 1 (2850–2400 m)	**1.0**	**1.5**	**2.0**	**2.5**
(spectrum from region I)	*97.4*	*88.8*	*76.6*	*63.4*
Layer 2 (2400–1800 m)	**4.3**	**4.5**	**4.7**	**5.0**
(spectrum from region II)	*19.7*	*17.0*	*22.5*	*18.8*
Layer 3 (1800–1250 m)	**5.5**	**5.7**	**6.0**	**6.4**
(spectrum from region V)	*16.1*	*20.4*	*17.7*	*20.3*
Layer 4 (1250–750 m)	**5.8**	**6.1**	**6.4**	**6.8**
(spectrum from region VII)	*36.8*	*36.2*	*42.1*	*38.5*
Final drop size	**5.9**	**6.2**	**6.5**	**6.9**
P (joint)	*1.1*	*1.1*	*1.3*	*0.9*
P' (joint)	*10.7*	*10.6*	*11.3*	*9.7*

tions were done for raindrops falling through layers of cloud bounded by the nominal elevation of each of the cloud passes. The initial drop sizes at the top of the uppermost layer were specified based on the range of large drop sizes observed during the highest cloud passes on 19 and 23 July. Drop sizes at the top of subsequent layers were determined from the accretional growth model discussed in the following paragraph. The raindrop size spectrum $C(d)$ was specified based on both 10- and 5-s raindrop spectra for 23 July (Fig. 4, Tables 2a and 2c) and 19 July (Fig. 8, Table 2c) measured within the rainshaft and centered on the large drop regions. The mean breakup time (t_b) for each drop size and cloud pass spectrum was calculated from Q'.

A simple accretion model was used to estimate the fall time (t_f) through a layer to account for the raindrop growth and increasing fall speed. The vertical profile of the cloud liquid water content used in the model in each case was based on the peak measured values of the liquid water content in the core of the observed updrafts. The fall velocity of the drop $V(t) = V_T(D) - W(z)$ was calculated using terminal velocities $V_T(D)$ determined from the drop diameter (Beard 1976) and assuming an updraft $W(z)$ profile based on the peak vertical velocities measured during the cloud passes. The measured raindrop spectrum at the level of each cloud pass was assumed to be representative of the layer immediately below.

In addition to the calculated survival probabilities for the drops falling through each layer, we calculated the joint probability for survival of each of the drops after passing through all of the layers (rows labeled P in Table 2). Because of the exponential change in P with n for small probabilities, we also recalculated the survival probabilities using the same drop spectra with one-half the concentration ($P' = e^{-n/2} = P^{1/2}$). These joint probabilities appear in the rows labeled P'.

The survival times of the large and giant drops were very sensitive to the concentrations of smaller raindrops within the main updraft. Size sorting (due to the difference in terminal velocities of the large and small raindrops) led to decreased concentration of small raindrops in the rainshaft containing the large and giant drops on 23 July, dramatically increasing the survival probabilities of the largest drops. Note further that on 23 July, the survival probabilities increased by a factor of 4 when 5-s spectra (representing the ~500 m wide region centered on the location of the largest observed drops) were used instead of the 10-s spectra (~1000 m wide region). The 19 July data showed no evidence of size sorting, and the survival probabilities of the larger raindrops were low (<2%). Because of high, uniform concentrations of smaller raindrops along the rainband, decreasing the averaging volume to 5-s spectra (not shown in Table 2) had virtually no effect on the survival probabilities of the large raindrops. The giant raindrops sampled on 19 July were in the lower part of the cloud (passes 5 and 6) and, just as in the 23 July case, occupied only a narrow (<500 m wide) region of the cloud. That may imply that on 19 July either the aircraft missed the center of the high reflectivity core (since, unlike on 23 July, the penetrations were along the rainband), or some other process of selection that we do not understand determined the location of the observed giant raindrops in the cloud. Data from both cases clearly illustrate that the concentrations of smaller raindrops in the middle and lower part of the cloud determine the cumulative survival probabilities of the large falling raindrops, since near cloud top, the survival probabilities are generally high (e.g., section c of Table 2) because of both the smaller size of the collector drop and the lower concentrations of raindrops with diameters ~1 mm.

In summary, the data from 23 July and calculations presented in Table 2 suggest that size sorting within the updraft core, due to difference in fall speeds of large and smaller drops, is an effective mechanism that decreases the concentrations of smaller raindrops, and the probability of large drop breakup. Size sorting can effectively promote the growth of giant raindrops and the development of high reflectivity cores. However, as the 19 July passes indicate, giant raindrops can exist in a less favorable environment with no direct evidence of size sorting. More data and better spatial and temporal resolution within the convective updraft regions are required to further our understanding of the correlation between collisional breakup and giant raindrop concentrations.

5. Conclusions

In this paper, we have documented the microphysical structure of the high reflectivity cores observed with radars offshore of Hawaii and have presented the results of calculations of raindrop growth and breakup probabilities within the high reflectivity regions. The key findings of these analyses are presented below.

1) Raindrops with diameters between 1 and 2 mm exist at cloud top during the developing stage of convective cells within Hawaiian rainbands.
2) Giant raindrops can grow from the 1–2-mm raindrops observed near cloud top by accretion of cloud water alone provided (i) updrafts are strong enough to suspend the 1–2-mm raindrops near cloud top where the most rapid growth occurs and (ii) the updrafts are not sheared significantly, allowing drops to remain in the updraft and high liquid water content regions during their fall through the cloud. The observations show that the requirements (i) and (ii) were met in narrow (~500 m wide) columns within the rainband cells. In other regions outside of the main updraft, drop size distributions were more exponential, with higher concentrations of small raindrops and no giant raindrops. Consequently, radar reflectivities and rainfall rates were lower. These regions of the rainbands, characterized by weak up-

drafts and downdrafts, are closer to an equilibrium state in which collisional breakup plays a more significant role in eliminating the large size tail of the spectra.

3) Size sorting due to differential terminal velocities of the larger and smaller raindrops that initially occurs in the updraft allows larger raindrops to fall through an environment in which there is a low concentration of smaller raindrops, significantly decreasing the probability of breakup.
4) High reflectivity cores in Hawaiian rainbands were associated with the giant raindrops present in narrow columns.

Although we have demonstrated that 1–2-mm drops near cloud top can grow to produce high reflectivity cores, the source of these raindrops could not be addressed with the aircraft data. We are currently addressing this issue by calculating raindrop growth along trajectories through both the three-dimensional Doppler kinematic fields obtained from HaRP and the high-resolution kinematic and thermodynamic fields generated by Clark's anelastic cloud model (Clark 1977, 1979; Clark and Farley 1984).

Acknowledgments. We thank everyone at the National Center for Atmospheric Research who contributed to the Hawaiian Rainband Project data acquisition and processing. We also thank Neil Laird at the Illinois State Water Survey and Jack Su at the University of Illinois for their contributions and L. J. Miller and Bill Anderson of the National Center for Atmospheric Research for their assistance with the radar data. Computing time was provided by the National Center for Atmospheric Research, which is sponsored by the National Science Foundation. This research was sponsored by the National Science Foundation under Grants NSF ATM 9020245 and NSF ATM 9223165.

REFERENCES

Austin, G., R. M. Rauber, H. T. Ochs III, and L. J. Miller, 1996: Trade wind clouds and Hawaiian rainbands. *Mon. Wea. Rev.*, **124,** 2126–2151.

Baumgardner, D., 1983: An analysis and comparison of five water droplet measuring instruments. *J. Appl. Meteor.,* **22,** 891–910.

Beard, K. V., 1976: Terminal velocity and shape of cloud and precipitation drops aloft. *J. Atmos. Sci.,* **33,** 851–864.

——, and H. T. Ochs, 1993: Warm-rain initiation: An overview of microphysical mechanisms. *J. Appl. Meteor.,* **32,** 608–625.

——, D. B. Johnson, and A. R. Jameson, 1983: Collisional forcing of raindrop oscillations. *J. Atmos. Sci.,* **40,** 455–462.

——, ——, and D. Baumgardner, 1986: Aircraft observations of large raindrops in warm, shallow, convective clouds. *Geophys. Res. Lett.,* **13,** 991–994.

Berry, E. X., and R. L. Reinhardt, 1974: An analysis of cloud drop growth by collection: Part I: Double distributions. *J. Atmos. Sci.,* **31,** 1814–1831.

Bowen, E. G., 1950: The formation of rain by coalescense. *Aust. J. Sci. Res.,* **A3,** 193–213.

Carbone, R. E., and L. Nelson, 1978: The evolution of raindrop spectra in warm-based convective clouds as observed and numerically modeled. *J. Atmos. Sci.,* **35,** 2302–2314.

——, J. Tuttle, W.-C. Lee, W. A. Cooper, and V. Grubisic, 1996: On the forcing of windward island rainfall in Hawaii. Preprints, *12th Int. Conf. on Clouds and Precipitation,* Zurich, Switzerland, ICCP, 494–497.

Clark, T. L., 1977: A small-scale dynamic model using a terrain-following coordinate transformation. *J. Comput. Phys.,* **24,** 186–215.

——, 1979: Numerical simulations with a three-dimensional cloud model: Lateral boundary condition experiments and multicellular severe storm simulations. *J. Atmos. Sci.,* **36,** 2192–2215.

——, and W. R. Farley, 1984: Severe downslope windstorm calculations in two and three spatial dimensions using anelastic interactive grid nesting: A possible mechanism for gustiness. *J. Atmos. Sci.,* **41,** 329–350.

Cornford, S. G., 1967: Sampling errors in measurements of raindrop and cloud droplet concentrations. *Meteor. Mag.,* **96,** 271–282.

Doviak, R. J., and D. S. Zrnić, 1993: *Doppler Radar and Weather Observations.* 2d ed. Academic Press, 562 pp.

Feller, W., 1957: *An Introduction to Probability Theory and its Applications.* Vol. 1. 2d ed. Wiley and Sons, 461 pp.

Gillespie, D. T., 1972: The stochastic coalescence model for cloud drop growth. *J. Atmos. Sci.,* **29,** 1496–1510.

——, and R. List, 1978: Effects of collision-induced breakup on size distributions in steady-state rain shafts. *Pure Appl. Geophys.,* **117,** 599–626.

Grubisic, V., P. K. Smolarkiewicz, R. M. Rasmussen, and R. E. Carbone, 1996: Hawaiian rainbands: Effects of thermal forcing on the rainband dynamics. Preprints, *12th Int. Conf. on Clouds and Precipitation,* Zurich, Switzerland, ICCP, 741–743.

Illingworth A. J., 1988: The formation of rain in convective clouds. *Nature,* **336,** 754–756.

Johnson, D. B., 1976: Ultragiant urban aerosol particles. *Science,* **194,** 941–942.

——, 1982: The role of giant and ultragiant aerosol particles in warm rain initiation. *J. Atmos. Sci.,* **39,** 448–460.

——, K. V. Beard, and D. Baumgardner, 1986: Airborne observations of raindrop distributions in Hawaiian clouds. Preprints, *Conf. on Cloud Physics,* Vol. 2, Snowmass, CO, Amer. Meteor. Soc., 48–51.

Knollenberg, R. G., 1972: Comparative liquid water content measurements of conventional instruments with an optical array spectrometer. *J. Appl. Meteor.,* **11,** 501–508.

Komabayasi, M., T. Gonda, and K. Isono, 1964: Lifetime of water drops before breaking and size distribution of fragment droplets. *J. Meteor. Soc. Japan,* **42,** 330–340.

List, R., and J. R. Gillespie, 1976: Evolution of raindrop spectra with collision-induced breakup. *J. Atmos. Sci.,* **33,** 2007–2013.

Low, T. B., and R. List, 1982: Collision, coalescence, and breakup of raindrops. *J. Atmos. Sci.,* **39,** 1591–1618.

McTaggart-Cowan, J. D., and R. List, 1975: Collision and breakup of water drops at terminal velocity. *J. Atmos. Sci.,* **32,** 1401–1411.

Ochs, H. T., and R. G. Semonin, 1979: Sensitivity of a cloud model to an urban environment. *J. Appl. Meteor.,* **18,** 1118–1129.

——, and D. F. Gatz, 1980: Water solubility of atmospheric aerosols. *Atmos. Environ.,* **14,** 615–616.

Owens, G. V., 1957: Wind tunnel calibrations of three instruments designed for measurements of the liquid water content of clouds. Tech. Note 10, Cloud Physics Laboratory, University of Chicago, 15 pp. [Available from Cloud Physics Laboratory, University of Chigaco, 5734 S. Ellis Ave., Chicago, IL 60637.]

Personne P., J. L. Brenguier, J. P. Pinty, and Y. Pointin, 1982: Comparative study and calibration of sensors for the measurement of the liquid water content of clouds with small droplets. *J. Appl. Meteor.,* **21,** 189–196.

Pruppacher, H. R., and R. L. Pitter, 1971: A semi-empirical determination of the shape of clouds and raindrops. *J. Atmos. Sci,* **28,** 86–94.

——, and J. D. Klett, 1997: *Microphysics of Clouds and Precipitation*. 2d ed. Kluwer Academic, 955 pp.

Rasmussen, R. M., P. K. Smolarkiewicz, and J. Warner, 1989: On the dynamics of Hawaiian cloud bands: Comparison of model results with observations and island climatology. *J. Atmos. Sci.,* **46,** 1589–1606.

Rauber, R. M., K. V. Beard, and B. M. Andrews, 1991: A mechanism for giant raindrop formation in warm, shallow, convective clouds. *J. Atmos. Sci.,* **48,** 1791–1797.

——, H. T. Ochs III, and J. Su, 1995: An analysis and visualization system for optical array probe data from instrumented aircraft. Preprints, *Conf. on Cloud Physics,* Dallas, TX, Amer. Meteor. Soc., 86–89.

Rogers, D., 1990: Raindrop trajectories to PMS probe on Electra. National Center for Atmospheric Research—Research Aviation Facility Internal Tech. Rep. [Available from NCAR-RAF, 1850 Table Mesa Dr., Boulder, CO 80307.]

Rogers, R. R., and M. K. Yau, 1989: *A Short Course in Cloud Physics*. 3d ed. Pergamon Press, 293 pp.

Saunders, P. M., 1965: Some characteristics of tropical marine showers. *J. Atmos. Sci.,* **22,** 167–175.

Smolarkiewicz, P. K., R. M. Rasmussen, and T. L. Clark, 1988: On the dynamics of Hawaiian cloud bands: Island forcing. *J. Atmos. Sci.,* **45,** 1872–1905.

Szumowski, M. J., R. M. Rauber, H. T. Ochs III, and L. J. Miller, 1997: The microphysical structure and evolution of Hawaiian rainband clouds. Part I: Radar observations of rainbands containing high reflectivity cores. *J. Atmos. Sci.,* **54,** 369–385.

Takahashi, T., 1978: Raindrop size distribution with collisional breakup in an axisymmetric warm cloud model. *J. Atmos. Sci.,* **35,** 1549–1553.

——, K. Yoneyama, and Y. Tsubota, 1989: Rain duration in Hawaiian trade wind rainbands—Aircraft observation. *J. Atmos. Sci.,* **46,** 937–955.

Telford, J. W., 1955: A new aspect of coalescence theory. *J. Meteor.,* **12,** 436–444.

——, 1975: Comments on ''Monte Carlo simulations of drop growth by accretion.'' *J. Atmos. Sci.,* **32,** 1638–1639.

Woodcock, A. H., 1952: Atmospheric salt particles and raindrops. *J. Meteor.,* **9,** 200–212.

——, 1953: Salt nuclei in marine air as a function of altitude and wind force. *J. Meteor.,* **10,** 362–371.